Open Research Online

The Open University's repository of research publications
and other research outputs

The cryptic summit graben of Mt. Etna volcano

Journal Item

How to cite:

Murray, John B. (2019). The cryptic summit graben of Mt. Etna volcano. Journal of Volcanology and Geothermal Research, 387, article no. 106657.

For guidance on citations see FAQs.

© 2019 Elsevier

https://creativecommons.org/licenses/by/4.0/

Version: Version of Record

Link(s) to article on publisher's website:
http://dx.doi.org/doi:10.1016/j.jvolgeores.2019.07.024

Copyright and Moral Rights for the articles on this site are retained by the individual authors and/or other copyright owners. For more information on Open Research Online's data policy on reuse of materials please consult the policies page.

oro.open.ac.uk

Journal of Volcanology and Geothermal Research 387 (2019) 106657

Contents lists available at ScienceDirect

Journal of Volcanology and Geothermal Research

journal homepage: www.elsevier.com/locate/jvolgeores

The cryptic summit graben of Mt. Etna volcano

John B. Murray

School of Environment, Earth & Ecosystem Sciences, The Open University, Walton Hall, Milton Keynes MK7 6AA, United Kingdom of Great Britain and Northern Ireland

ARTICLE INFO

Article history:
Received 22 January 2019
Received in revised form 31 May 2019
Accepted 31 July 2019
Available online 1 August 2019

Keywords:
Volcano structure
Gravitational spreading
Eruptive mechanism
Ground deformation
Volcano geophysics

ABSTRACT

Previous studies have inferred the likelihood of a summit graben at Mt. Etna, but until now there has been no direct observation or evidence of such a feature. Here, the results of 43 years of deformation measurements at the summit are reported, in which the presence of an actively forming north-south graben 1.5 km wide is evident, with a maximum subsidence of nearly 4 m in 43 years. Its bounding faults have in most places been hidden by the eruptive deposits of 190 summit eruptions, but horizontal measurements across these faults show a maximum value of nearly 9 m of east-west extension. Most of the subsidence and extension has taken place during the injection of eruption feeder dykes, with extreme values for single events of −1.7 m subsidence during the injection of the 2002–2003 dyke, and 4.4 m extension across the 1989 feeder dyke, but subsidence and extension continues to take place slowly during inter-eruptive periods. Analogue modelling indicates that its origin is probably a consequence of the gravitational spreading and downslope sliding of the Etna edifice on its clay-rich substrate, aided by magmatic pressure from feeder dykes intruded into individual faults, and by downward pressure from surface loading of erupted lava. This study clarifies the way in which the mechanism of gravitational spreading is maintained throughout the lifetime of this and other spreading volcanoes and rifts on Earth and Mars.
Crown Copyright © 2019 Published by Elsevier B.V. This is an open access article under the CC BY license (http://creativecommons.org/licenses/by/4.0/).

1. Introduction

Etna is the type specimen of a gravitationally spreading volcano, in which extensional structures at the summit are a consequence of outward gravitational spreading of the flanks (Borgia et al., 1992; Borgia and Murray, 2010; Merle and Borgia, 1996). But although north-south eruptive fissure traces predominate in the summit region, there have been no reports of overall cumulative subsidence at the summit. The long record of deformation measurements at Mt. Etna means that secular vertical deformation of the upper parts of the volcano can in many places be determined with millimetre accuracy back to 1975 (Murray et al., 1977), and horizontal deformation from about 1981 onwards (Murray and Pullen, 1984) for the southern flank, and from about 1987 for the whole summit area (Murray, 1994). Examination of the entire deformation record August 1975 – September 2018 reveals the existence of a graben with a floor that is sinking continuously, and bounding faults that are extending at variable rates.

The existence of this graben appears to have escaped notice partly because the fractures associated with its formation have been rapidly covered by up to 120 m of ash and lava from this most active volcano (Murray, 1980; Behncke et al., 2006), but also perhaps because during the four decades for which data is available, it has subsided piecemeal rather than as a single unit, though the edges are well-defined on the map of cumulative movement. It has been undetectable by radar interferometry, because Etna's summit area lacks permanent scatterers (Bonforte et al., 2011).

2. Methods

2.1. Field measurements

This paper is the result of 63 trips to measure ground deformation at Etna over 43 years. The principal method used to obtain vertical deformation data has been precise levelling begun in 1975, which has a mean accuracy of 1.6 mm√K at Etna, where K is the distance levelled in kilometres. The techniques of streamlined levelling used on Etna are described in detail in Murray et al. (1995). A Zeiss Ni2 self-levelling level, 0.5 mm micrometer and 3 m invar staff were used 1975–1991, since when a Leica Na2000 digital level and 3 m invar barcode staff have been used. The traverse is not double-run; accuracy is determined from closed loops of up to 69 km, and varies from 0.04 mm√K when the volcano is quiet to 4.0 mm√K when the volcano is deforming during eruptions. This is by far the most accurate method, but is a slow and difficult process except on vehicle tracks and roads, so trigonometric levelling was used to access the Valle del Bove and other remote areas from 1983 onwards. Where more than one method was used to measure the same point during the same trip, the result of the most accurate method was used. Horizontal deformation data is available from 1981, when a trilateration network was installed by A.D. Pullen (Murray and Pullen, 1984) and measured with Electronic Distance Meters (EDM) and theodolites (later total stations), and

E-mail address: j.b.murray@open.ac.uk.

https://doi.org/10.1016/j.jvolgeores.2019.07.024
0377-0273/Crown Copyright © 2019 Published by Elsevier B.V. This is an open access article under the CC BY license (http://creativecommons.org/licenses/by/4.0/).

continued until 1994. This was superseded by a large dual-frequency GPS network installed 1989–1995, and trigonometric levelling was finally abandoned in 1998. A dry tilt network was installed 1975–1982 and provides important information on lower flank movements prior to the advent of GPS, and for continuity's sake is still measured. Today the deformation networks comprise 322 levelling benchmarks, 100 GPS stations measured with Leica dual frequency System 500 kits, and 27 dry tilt stations.

These are the remnant of >1400 levelling, trilateration, GPS and dry tilt stations that have been installed over the years, more than two-thirds of which have been lost under lava or ashfalls, removed by tourists, bulldozed during road works or rusted away. The vast majority of the benchmarks are steel road nails used in levelling, which are installed in solid lava outcrops. Those near the summit disintegrate from serious rusting after as little as 30 years, but these have been steadily replaced by new stainless steel nails, usually in the same outcrop, and the two measured concurrently until the old nail disintegrates entirely. Some stainless steel stations were installed in 1976, and these remain pristine after 42 years. All stations are deliberately hidden beneath rocks, as 26% of them disappeared in the first year and a further 9% in the second year, though this decreased to negligible amounts as soon as the nails became rusty (Murray et al., 1995). Witness nails for many benchmarks were installed from the start, so that when a benchmark is lost it can be replaced, and its height relative to the old nail known to a fraction of a millimetre. For access to raw data, please apply to the author.

2.2. Other deformation networks

At least 5 other individuals or organisations have installed deformation networks before or during the period 1975–2018 covered here. Wherever possible, stations from other networks were incorporated or tied in to the original 1975 levelling network and its extensions, so that the networks could in the future be linked if necessary. In 1837–1843, Sartorius von Waltershausen (1880) surveyed the whole of the Mt. Etna massif, installing a large number of trigonometric points for triangulation. Although his survey was of low accuracy by today's standards and not intended for deformation work, these points, at least 6 of which survive today, may nonetheless become important when values of secular deformation start to exceed the error ellipses. Two of them are now routinely measured each year. Similarly, one station from the Istituto Geografico Militare (I.G.M.) survey (1868, 1932) is measured every year.

In 1971, Geoff Wadge (1976) installed 3 dry tilt stations and a network of 19 stations around the summit craters to measure horizontal strain with electronic distance meters 1971–1974. 13 of his stations were incorporated into the original levelling traverse of 1975, and 4 of these are in use today.

Lettario Villari (1977, 1983) installed 3 similar networks 1976–1978 to measure strain lower down the edifice on the western, northeastern and southern flanks, though unfortunately the 3 networks were not tied together. Two of his stations were incorporated into the levelling traverse.

In 1980, the Vesuvius Observatory installed a 35 km precise levelling network around the flanks of the volcano that was not connected to the summit levelling traverse, nor to the dry tilt stations that lie along the levelling route. This Flank Levelling Traverse began at Monti Silvestri, 2 km to the south of the southernmost station of the summit traverse and 600 m below it in altitude. It ran into the Forestry track past Monte Denza up the western side to Monte Spagnolo in the northeast, and across past Grotta dei Lamponi to the Pernicana Fault in the northeast (Sanderson et al., 1983). It was later extended a further 5 km southeastwards from Monti Silvestri, and to Citelli in the northeast and eventually to the Monti Peloritani at the north foot of Etna (Obrizzo et al., 2001). This levelling traverse is today connected to the summit network by precise levelling down the north and south flanks, to create a network of connected levelling lines >100 km long, routinely measured in about 19 days. 8 dry tilt stations were installed by the same organisation, some in similar locations to those of the pre-existing dry tilt network. Three of these have been tied into the levelling traverse since.

A.D. Pullen established a trilateration network of 30 stations on the south flank in 1981, from Monte Denza to the Schiena del Asino, which included the 8 surviving stations of Wadge's summit network (Murray and Pullen, 1984). Vertical angles were also measured, which meant that Pullen's network could be used as a trigonometric levelling traverse to derive vertical as well as horizontal deformation. Using this data, the summit levelling network could be linked to the flank levelling line for the first time, at Pullen's Mt. Denza station. Six of his stations were incorporated into the levelling traverse, and today eleven stations from his original 1981 stations are measured annually as part of the GPS network. In 1983, three trigonometric levelling lines were set up to connect the summit levelling traverse to the Flank levelling traverse in the south, west and north, and also to reach Monte Centenari in the Valle del Bove.

The first GPS measurements were made by Pierre Briole, Jean-Claude Ruegg and members of the French IPGP in 1988, when a 9 station network was installed of much greater extent, that included two stations off the volcano altogether (Briole et al., 1992). Two of these stations were tied into the levelling network. This was followed in 1989 by a similar rudimentary GPS network of 6 stations, primarily used to orient and fix the trilateration network (Sargent and Murray, 1994), and the INGV Catania began to expand their 1988 network (Nunnari and Puglisi, 1994). As GPS satellite numbers increased, both these networks were increased in size, and have continued to do so over the past 30 years. The network operated by the INGV Catania now comprises about 30 continuously-recording GPS stations (Bonforte and Guglielmino, 2015). Four INGV stations are measured annually as part of the GPS network, and several others are measured occasionally.

2.3. Data processing

2.3.1. Station loss

Only 17 of the original levelling benchmarks measured in 1975 were still extant in 2018, though within this period of time 69 other stations have survived for periods of 35 years or more. To extend the coverage to 43 years, stations were tied in to earlier or later stations by witness nails close by, or if lost under lava flows, to the nearest benchmarks on either side of the flow.

2.3.2. Dry tilt stations

No levelling below 2300 m altitude was carried out before 1980, but in 1975–1976 a network of 39 dry tilt stations was installed over the entire edifice, 16 of which have survived intact and are measured annually (see Fig. 1). Where tilt is fairly constant in direction, it has been used to deduce altitude changes with reference to nearby levelling stations by matching measured tilt to measured altitude change. For example, the Punta Lucia dry tilt station (see Fig. 1), which was linked by levelling to nail N in 1987 for the first time, tilted 616 μ towards the nail between 1987 and 2018, during which time the levelling station sank 0.45 m relative to the dry tilt station. On this basis, we deduce a mean equivalence of 1362 μ tilt to 1 m subsidence. Since the tilt at Punta Lucia 1976–2018 was 2661 μ, we estimate that N station subsided about 2 m relative to Punta Lucia 1976–1987. Applying the same procedure to the tilt vectors of dry tilt stations on the flanks, seen around the periphery of Fig. 1, indicates that between 1975 and 1980, flank deformation was restricted to small random movements, with no build-up of deformation in any sector (Murray and Guest, 1982).

2.3.3. Trigonometric levelling

Instead of using a level, which only sights horizontally and so restricts measurement to shallow slopes and distance of no >30 m per set-up, trigonometric levelling uses theodolites, which can measure at

any angle. This means that it can measure up very steep slopes, across valleys and dangerous terrain to distances of up to 1 km. The technique is carried out with two teams measuring vertical angles with theodolites and EDMs, one team at each end of each line to be measured. A series of four vertical angles (two pairs of face right and face left readings) are then read simultaneously theodolite to theodolite. Six distances are then measured with a distance meter at one end and a reflector at the other. Vertical height differences are derived from simple trigonometry, taking the mean of the vertical angle as the elevation angle and the mean of the measured distances as the hypotenuse. Subtracting instrument heights at both ends of the line gives the geodetic height difference between the two points. The first team then moves forward past the second team to the third point, where the process is repeated, this time looking back from the third point to the second team on the second point. The second team then moves forward past the first team on to the fourth point and the process is repeated. The two teams continue in this way, leapfrogging each other until the final point in the trigonometric levelling line is reached. The two teams then change places and restart the process, this time moving back measuring from point to point until the first point to be measured is reached. This provides two independent measures of relative height for each point, the difference between the two providing a closing error from which the precision can be deduced.

2.3.4. Trilateration

Trilateration uses the same instruments, and the same procedures as trigonometric levelling. Instead of a simple line of points however, a network of points is measured, ideally laid out as a series of roughly equilateral triangles. Each line between adjacent points is measured, so ideally six or more lines will be measured from each point. The process is continued until every line in the network has been measured. To derive relative horizontal coordinates, additional processing to that for trigonometric levelling is required. Positions of points were derived by standard procedures using STAR*NET-PRO version 6.0.25, the error ellipses for each point being derived from multiple redundancy in the network.

2.3.5. GPS data incorporation

For levelling and trigonometric levelling, both methods give results as geodetic heights, so no additional data processing is necessary to tie networks together. However, with the advent of dual-frequency GPS, which gives results in ellipsoidal coordinates, information on the local geoid is needed to convert them to geodetic heights. Accordingly in 1994, at the changeover from geodetic methods to GPS, stations were measured with both GPS and geodetic surveying instruments. The height difference between geodetic and ellipsoidal results for each point was plotted to make a detailed map of the geoid on Mt. Etna. Extreme values show that altitudes measured by GPS give values more than a metre higher northwest of the summit near Punta Lucia than they do at the lower right corner of the map in Fig. 1. The geoid map has continued to be refined, as many levelling stations are also measured annually with GPS, some points having been re-measured simultaneously by both methods up to 23 times since 1995.

These continued difference measurements give standard deviations averaging ± 0.02 m, with extreme values of ± 0.04 m, indicating, as a by-product, a lower accuracy for GPS than for levelling, but sufficient for this study.

2.3.6. Horizontal coordinates prior to GPS

All the strain and trilateration networks prior to 1988 used different base stations, and different base orientations. The base station was usually chosen as the furthest from the summit, and the orientation defined by taking the orientation of one of the measured lines as fixed. When GPS measurements were first carried out, the network orientation was derived from the measurements themselves, and true positions could for the first time be derived by tying in to the Continuously Operating Reference Stations (CORS) of the International Terrestrial Reference Frame (ITRF). Since the present study includes data from before the GPS era, horizontal deformation is presented only in terms of the changing length of distances measured between two stations, rather than vectors of movement for individual stations.

3. Results of field measurements

Regarding the vertical data, a map showing contours of vertical displacement is shown in Fig. 1. The map has largely been assembled with reference to earlier publications (Murray et al., 1977; Murray and Guest, 1982; Murray and Pullen, 1984; Murray, 1988; Murray et al., 1989; Murray, 1990; McGuire et al., 1991; Rymer et al., 1993; Murray et al., 1994; Murray, 1994), updated with more recent unpublished data. Contour interpolation has been carried out by hand, with the aid of contemporary surveys of cracks and faulting associated with dyke injection. These surveys were in most cases carried out by detailed tacheometry (e.g. Murray, 1980), or in remote areas by resection of critical points. In many cases, limits of areas of subsidence are clearly marked by the surface traces and configurations of fracture fields, faults and their downthrow, e.g. the 1986 Sep 24th intrusion (Murray et al., 1989). Later positions of fracture fields from the 1989, 2001, 2002–3 and 2008–9 eruptions, mapped by Ferrucci et al. (1993) Neri et al. (2004), Lanzafame et al. (2003) and Bonaccorso et al. (2011), also aided in the contouring of deformation associated with these eruptions, as did observations of fault locations and movement of the Pernicana Fault by Ruch et al. (2013). Where stations or witness stations have lasted for a combined total of 30 years or more, no pro rata increase in movement is added. Stations with <30 years' data have been used in combination with fault and fissure maps to decide whether such a pro rata increase is justified. Further details in the Supplementary Material.

The most striking feature in Fig. 1 is the deep sigmoidal graben running from south to north across the summit. In the 43 years 1975–2018, the centre of the graben has sunk by nearly 4 m in the north-central section that lies across the summit of the volcano. The contour of 2 m subsidence extends from the Piano del Lago in the south to the Northeast rift, where it merges with the subsiding Pernicana fault (Obrizzo et al., 2001), creating a graben >7 km long and 2 km wide at its widest point.

Station 77, north of the summit, is in the area of highest subsidence, and has subsided 3.62 m in 43 years. A station 220 m west of it subsided 3.80 m, and shorter-lived stations nearer the summit are likely to have subsided more than this. For example, a station on the rim of the Southeast Crater subsided 0.38 m in two years between 1987 and when it was destroyed in the 1989 eruption, and another installed in 1990 to replace it subsided 1.72 m in the six years 1990–1996 when it too was destroyed, a combined total of 2.1 m subsidence in only 8 years. There are other stations at the summit which showed similar large subsidence over a few years before being destroyed, and summit contours of deformation in Fig. 1 should be regarded as conservative values, the subsidence being possibly greater than shown.

The map in Fig. 1 indicates that nearly all the upper half of the volcano has shown overall subsidence. A few small slivers of land around the south end of the graben have been uplifted by 5 to 30 cm, and also in the Valle del Leone, where one station was uplifted by more than a metre during the 1989 eruption (Murray, 1994). The edges of the graben show some subparallel offshoots mainly corresponding to the traces of eruptive dykes; more of these have doubtless been missed to the northwest (1981 eruption) and on the eastern and southern sides (2008–9 and 1991–3 eruptions) due to paucity of benchmarks in these areas.

3.1. Time variation in the rate of subsidence

The vertical movement in time is presented in two ways. Fig. 2 shows the east-west ground tilt measured at a dry tilt station at the west (Punta Lucia) and east (Portella Giumenta) edges of the graben.

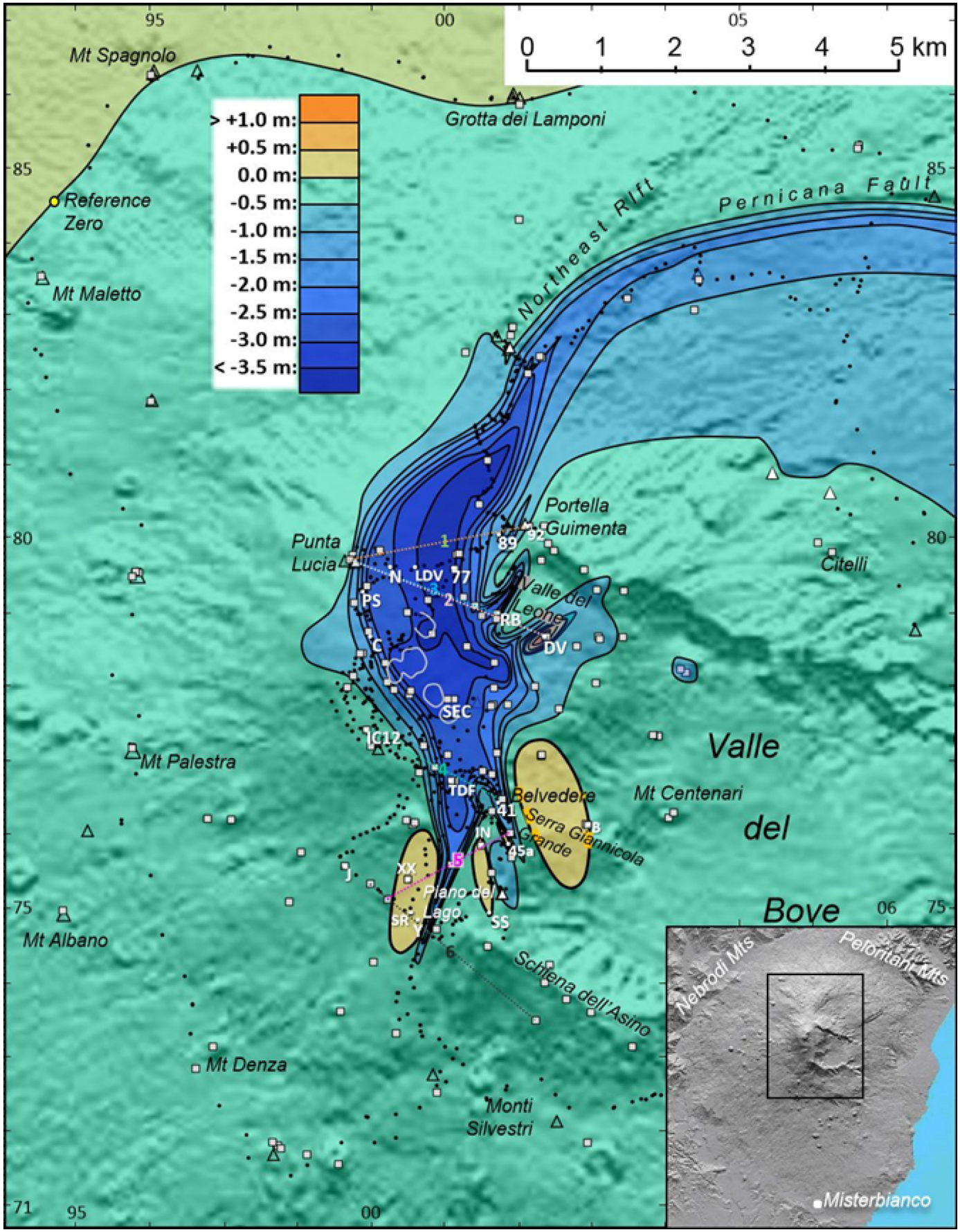
95
00
05
0 1 2 3 4 5 km
Mt Spagnolo
Grotta dei Lamponi
> +1.0 m:
+0.5 m:
0.0 m:
-0.5 m:
-1.0 m:
-1.5 m:
-2.0 m:
-2.5 m:
-3.0 m:
< -3.5 m:
85
Reference Zero
Mt Maletto
Northeast Rift
Pernicana Fault
Portella Guimenta
Punta Lucia
80
Citelli
Valle del Leone
Mt Palestra
Valle del Bove
Mt Centenari
Belvedere Serra Giannicola Grande
Piano del Lago
Mt Albano
75
06
Schiena dell'Asino
Mt Denza
Monti Silvestri
71
Nebrodi Mts
Peloritani Mts
Misterbianco
N
LDV
PS
C
RB
DV
SEC
IC12
TDF
IN
XX
SR
SS
B
89
92
77
41
45a

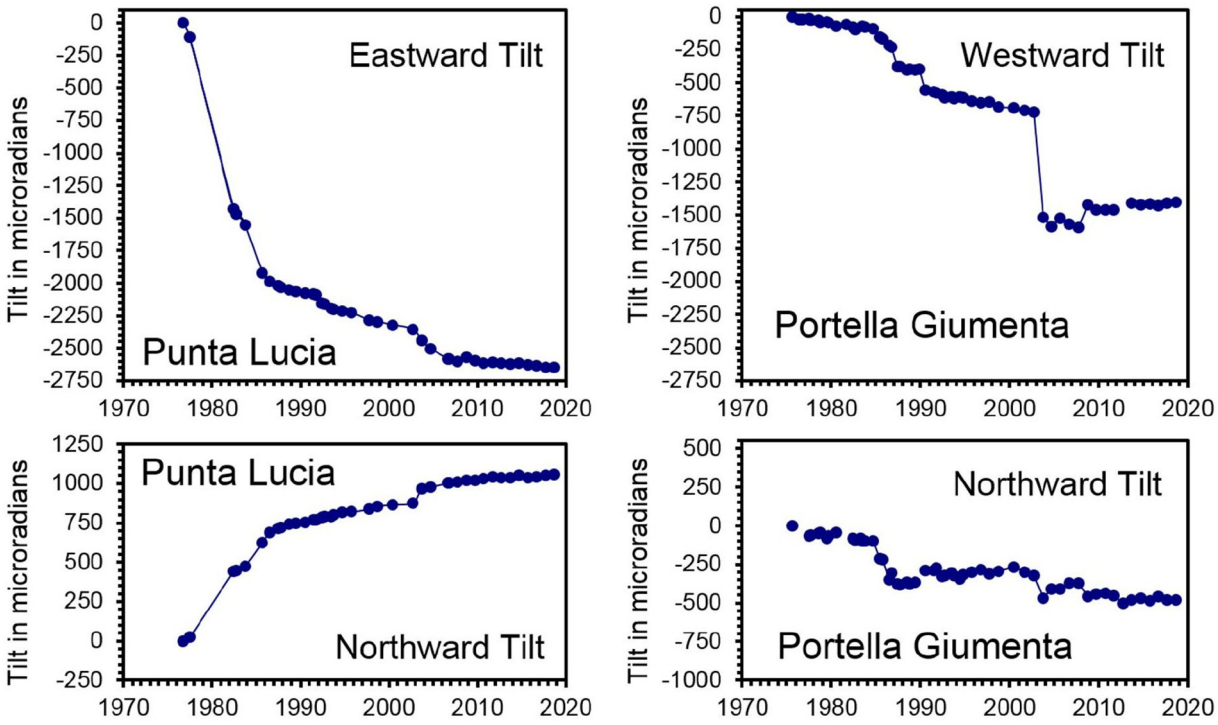

Fig. 2. East-west (top) and North-south (bottom) ground tilt measured at the west (left) and east (right) edges of the graben. Locations are shown in Fig. 1.

At the west side, most of the subsidence occurred between 1975 and 1985, in which period the ground tilted eastwards by >2000 microradians (μ), whereas at the eastern edge the main movement occurred during the 2002–3 eruption, when the ground tilted west by 700 μ in one event. Both sides show slight recovery during the 2008–9 eruption.

Fig. 3 shows plots of the amount of subsidence versus time in different parts of the graben (station locations given on Fig. 1), relative to a station at Portella Giumenta, just east of the subsiding zone. It clearly demonstrates that subsidence has occurred at different times in different parts of the graben. North of the summit, subsidence of 1 to 2 m occurred in the decade 1975–1985, mostly during the 1981 and 1985 eruptions. There was then a slower subsidence rate of around 0.1 m per decade 1985–2002, followed by an abrupt subsidence during the 2002–3 eruption of up to 1.7 m in the central and eastern part of the graben, and then a drop of 0.8 m during the 2008–9 eruption in the centre of the graben only, since when the subsidence rate has reverted to around 0.1 m per decade.

South of the summit, things have been different. Subsidence here has only occurred during fissure eruptions: about 0.6 m during the 1983 eruption, 0.5 m during the 1991–3 eruption at Station 41 (Belvedere) only and 1.2 m during the 2001 and 2002–3 eruption at the Torre del Filosofo (TDF) only. Between these times, there has been little or no subsidence. Indeed, uprise has occurred between 1985 and 1990 (0.1 to 0.3 m), and at Belvedere during the 2001 and 2002–3 eruptions (0.2 m). The only exception is the period 2013 to 2017, when a station near the Torre del Filosofo subsided 0.40 m, after the original station had been overcome by lava in 2013.

Overall, it is clear that at least 70% of graben subsidence occurred during dyke emplacement associated with eruptions, and also that south flank subsidence has been unaffected by north flank eruptions, with the possible exception of the 1981 eruption, when the south flank dropped about 0.1 m. Similarly, the north flank is generally unaffected by south flank eruptions, apart from one minor (1991–3) and one major exception (1985), the latter accompanying a subsidence of up to 0.28 m near the northwestern edge of the graben (Murray, 1990).

3.2. Horizontal extension across the graben

Information on horizontal displacements dates from 1981 (Murray and Pullen, 1984) for the south flank, and 1987 for the north flank, though Bonaccorso (1999) has modelled measurements made by Villari (1983) which allows approximate movements to de deduced back to 1980 on the north side.

Fig. 4 shows these displacements plotted against time, in the form of changing line lengths across the graben. The position of each line is shown by the coloured dotted lines in Fig. 1. The biggest increases are 6.8 m on the south flank and 8.7 m on the north flank. The 8.7 m increase is at line 2, which runs from Punta Lucia at the west side to DV station in the centre of the Valle del Leone. DV lies 100 m east of the 1989 eruptive fissure and underwent a 4.42 m horizontal displacement during that eruption (Murray et al., 1994). Line 3 virtually overlies line 2, but stops at the edge of the main graben at the head of the Valle del Leone (Station RB). It shows similar increases to lines 1 and 2, apart from the 1989 event. Increases occur abruptly during the 2002–3 and 2008–9 eruptions, and lines 2 and 3 show small increases of 0.25 and

Fig. 1. Map showing contours of vertical ground deformation at Mt. Etna during the 43 years August 1975–September 2018. The reference zero is north of Monte Maletto at top left, 8 km northwest of the summit and 1850 m below it. Black dots indicate levelling stations, white squares denote three-dimensional measurement stations (trigonometric levelling, trilateration and later dual-frequency GPS), and open triangles Dry Tilt stations. Coloured dotted lines show the locations of lines 1 to 6 shown in Fig. 4, and alphanumerics the stations in Fig. 3. Summit craters are outlined in grey, and edge ticks show UTM coordinates in kilometres. The inset (lower right) shows the map location with respect to the rest of the Etna massif. (For interpretation of the references to color in this figure legend, the reader is referred to the web version of this article.)

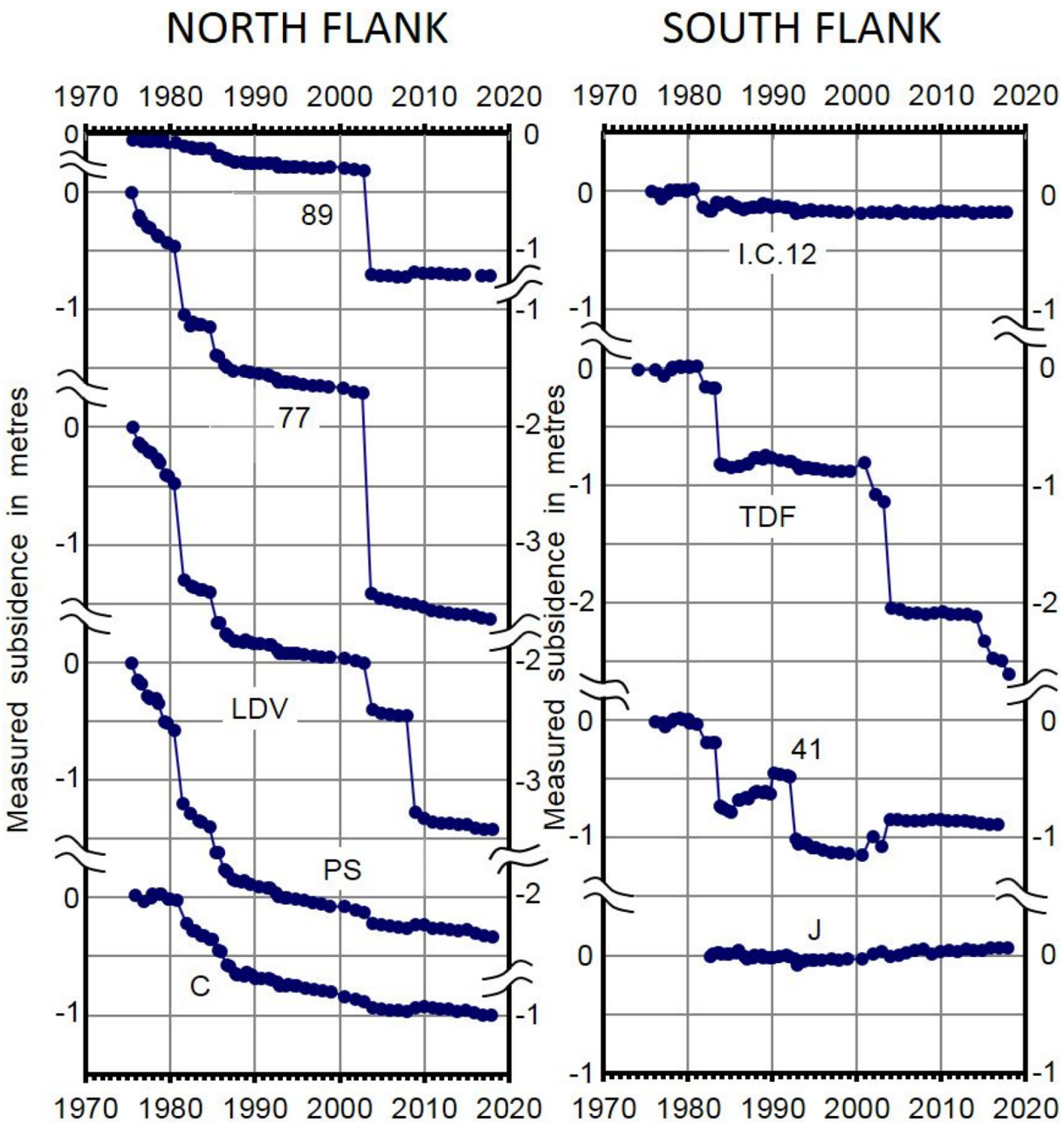

Fig. 3. Vertical displacements measured at stations north (left) and south of the summit (right) between 1975 and 2018, locations are shown in Fig. 1. N.B. a different reference zero is used from that in Fig. 1, at Portella Giumenta, east of the subsiding area. Periodic levelling down to the Fig. 1 reference shows that this may cause differences of about 0.1 m for some stations. All stations above lie within the main area of subsidence except I.C.12, which lies about 1 km southeast of the summit, and station J, which lies about 1 km west of the southernmost part of the subsiding area. The most recent 4 measurements at TDF (Torre del Filosofo) station are from a witness station nearby, since TDF was submerged under lava in December 2014.

0.35 m during the 2001 eruption, which are not shared by line 1. Lines 4 and 5 on the south flank also show an increase of 0.40 to 0.89 m during the 2001 eruption, and 1.63 and 1.74 m during the 2002–3 eruption. Even line 6, beyond the southern limits of most of the deformation shown in Fig. 1, shows a combined movement for both eruptions of 1.39 m (1997–2005). Similar increases are possible during the 1991–3 eruption, and possibly the 1983 eruption too for line 5, but lines on the south flank were measured too infrequently during this period to be sure.

3.3. The summit graben prior to 1975

How representative of Etna's past behaviour and history is the period covered by this study? The positions and orientation of eruptive fissures 1975–2018 have been to the northwest (1975, 1981), on the northeast rift (2002−3), to the east and northeast (1979, 1985, 1986–7, 1989, 2001, 2008–9, 2014), to the southeast (1978, 1991–3), and on the southern rift (1983, 1985, 2001, 2002–3). These are all of similar position and orientation to eruptive fissures which opened 1600–1974, and also to prehistoric fissures and vents. The only zone not active during the past 43 years is the western vent area, in which the 1651, 1763, 1832, 1843 and 1974 eruptions occurred (Guest and Murray, 1979).

Is there any evidence for the existence of a summit graben before these measurements began in 1975? Examination of the first accurately contoured maps of the volcano published in 1932 by the Italian Istituto Geografico Militare (I.G.M.) show a well-defined east-facing scarp up to 25 m high running northeast from Punta Lucia, now almost entirely

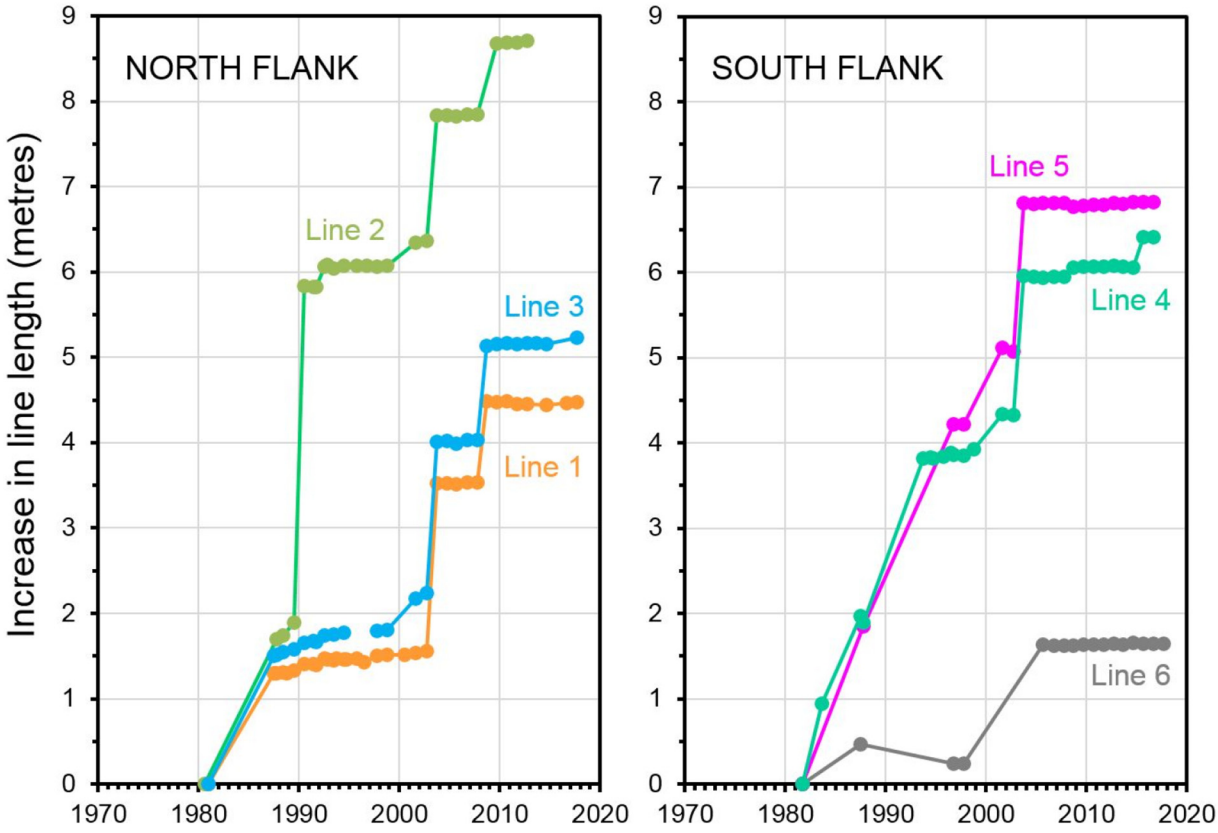

Fig. 4. Graben opening portrayed by increasing line length between stations east and west of the graben 1980–2018. Position of each line is shown in Fig. 1. Values are from trilateration measurements 1981–1994, and dual-frequency GPS 1994–2018. The north flank values (lines 1, 2 & 3) for 1980 are derived from the 1980–81 displacement model in Bonaccorso (1999). The displacements 1980–1987 for these lines should be regarded as minimum values, as they do not include possible displacements during the 1983, 1985 and 1986–7 eruptions. Elastic modelling of these latter eruptions (Murray and Pullen, 1984; Murray, 1990) suggests that such displacements would be negligible for the 1983 and 1986–7 eruptions, but up to a possible 0.1 m for the 1985 eruption.

submerged beneath 1968–1981 lavas. A west-facing feature of similar height can be seen at the other edge of the graben, running north-south <1 km northwest of the Portella Giumenta, now mostly covered by 1962–1966 lavas. These scarps are consistent with the position and shape of the graben shown in Fig. 1 north of the summit, and the implied subsidence of 25 m indicates over 400 years of subsidence at present rates. Even in the 1932 map, the foot of the well-defined scarp on the west side is submerged beneath 1838 and May 1923 lavas, indicating that the scarp may have been higher prior to these eruptions, so that subsidence at present rates could have been going on longer than 400 years. The rest of the summit area preserves little evidence of the graben even on the 1932 map, but with frequent summit eruptions of ash and lava occurring throughout historic time (Tanguy, 1981), fault scarps are liable to have been obscured soon after they were formed, as has occurred during the 43-year period under study here. Prior to about 1740 there was no summit cone of Etna, only a gently inclining plain about 3 km diameter with a broad, deep pit in the centre, which by 1769 had been submerged under an already substantial summit cone (Hamilton, 1770), implying a high resurfacing rate which would have hidden all traces of a graben. South of the summit area, no distinct scarps or other traces of the graben can be seen in the 1932 map.

4. Laboratory analogue modelling

Murray et al. (2018) demonstrated that the entire Mt. Etna edifice, constructed on a sloping basement (Branca and Ferrara, 2013), is moving downslope. To investigate the effects of this downslope movement combined with the gravitational spreading of the edifice, and whether this combination of forces might produce a summit graben, analogue experiments were carried out similar to those of Merle and Borgia (1996) and Wooller et al. (2004).

4.1. Model set-up

Laboratory models were constructed in which the sedimentary basement beneath Etna is represented by a layer of silicon putty, which is a ductile material that flows slowly (Merle and Borgia, 1996). The model set-up is shown in Fig. 5. A sand barrier was constructed around the silicon putty to allow it to form a horizontal surface, which takes 8 to 10 h. The silicon putty surface is then covered with a sand layer, to represent the apron of lavas that cover the lower slopes of Etna. The sand deforms as a brittle material. A sand and plaster cone, representing the main summit edifice of Etna, is then constructed on the sand, and the entire model is tilted 2° towards the right, the tilt of Mt. Etna's basement slope. The sand barrier is then removed from the downslope side of the model, to allow the silicon putty to flow downslope, as happens on the east slope of Etna. Cone height, cone position, lava apron thickness, basement thickness and basement slope angle were chosen to match those at Mt. Etna. The remaining sand barrier around the rest of the model corresponds to the hills surrounding the north (Peloritani), west (Nebrodi) and south (hills south of Misterbianco) of Etna.

4.2. Scaling analysis

Selected geometric variables are shown in the cross section of the model (Fig. 5, top), and with material properties are listed in Table 1. Geometric variables include the sand cone height (H_v) and radius (L_v),

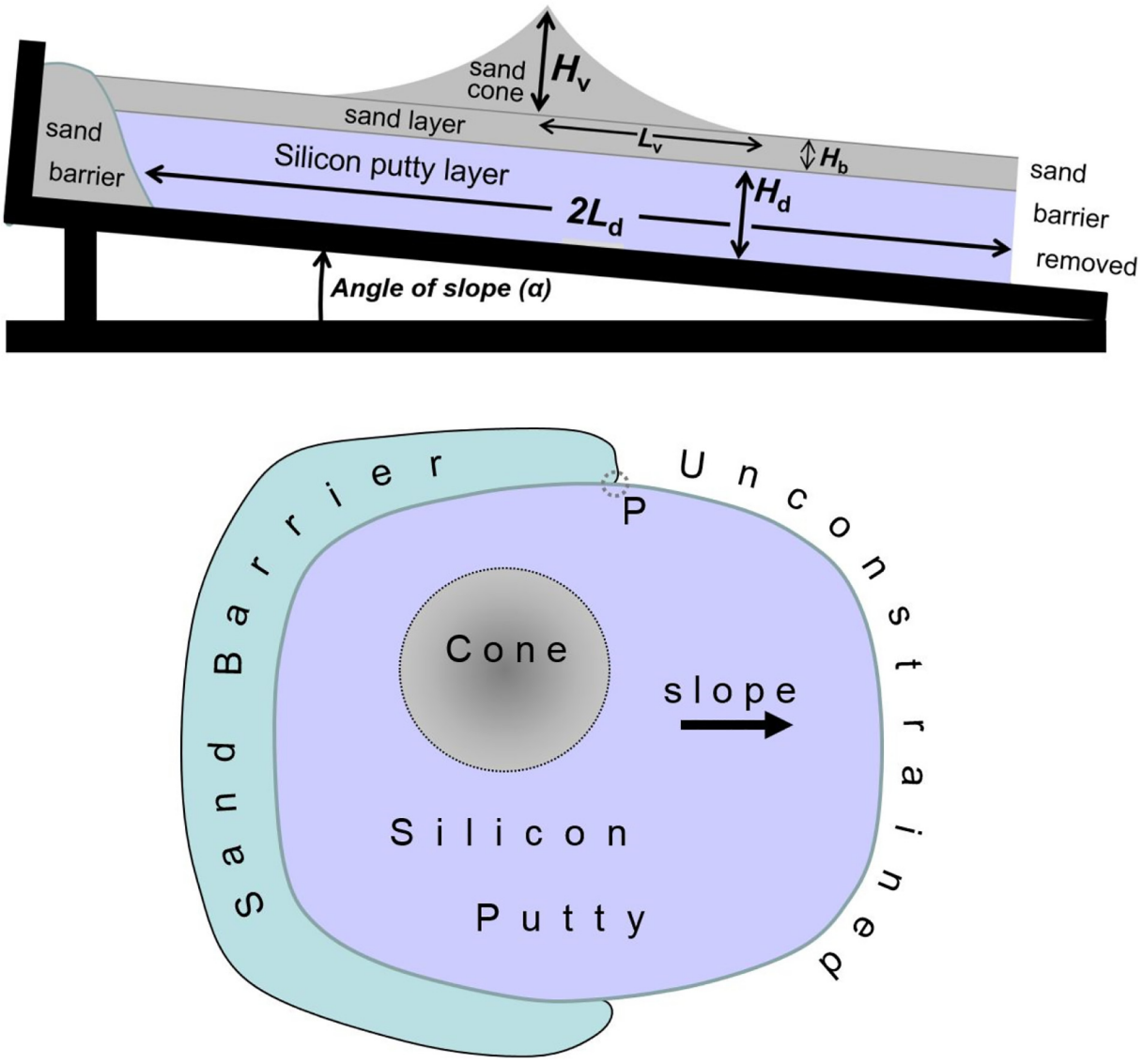

Fig. 5. Analogue model set-up showing cross section through apparatus (top) and plan view (bottom). In the plan view, the cone is placed assymetrically upon the silcon putty to match the situation at Mt. Etna (Fig. 1 inset) where the cone is closer to the Monte Peloritani to the north. Similarly the silicon putty extends further on the right side, to mimic the unconstrained slope on this side that continues beneath the Mediterranean Sea.

Table 1
Values for the geometric variables and material properties (defined above in Section 4.2) in nature and the analogue laboratory experiments. Where two values are given for the laboratory experiments, these refer to the model shown on the left and right respectively of the two models in Fig. 6.

Variable	Units	Etna	Laboratory	
H_v	m	1600	0.045	0.045
L_v	m	6000	0.15	0.19
H_b	m	700	0.02	0.02
H_d	m	>89	0.012	0.014
L_d	m	32,000	0.42	0.37
α	degrees	2°	2°	
ρ_v	kg m^{-3}	2500	1400	
ρ_b	kg m^{-3}	2500	1400	
ρ_d	kg m^{-3}	1900	1000	
Φ	degrees	35°	35°	
μ_d	Pa s	10^{19}	2×10^5	
g	m s^{-2}	9.81	9.81	
T	s	10^{12}	2.6×10^3	2.4×10^3

the thickness of the sand layer (H_b) and silicon putty layer (H_d), the radius of the silicon putty layer (L_d) and the angle of substrate dip (α). Material properties include the densities of the sand cone (ρ_v), the sand layer (ρ_b) and the silicon putty layer (ρ_d), the angle of internal friction of the sand (Φ), and the viscosity of the silcon putty (μ_d). The force of gravity (g) is included, and the time span of deformation (T). The scaling method of Merle and Borgia (1996) is used, but with an extra term for substratum slope introduced by Wooller et al. (2004). The laboratory variables scale up to those on Mt. Etna within the uncertainty of the latter values.

Etna values for H_b and H_d are derived from Branca and Ferrara (2013); other properties from Wooller et al. (2004) and Merle and Borgia (1996).

4.3. Analogue modelling results

The experiments produced a summit graben with similar shape, orientation and relative width to that at Etna (Fig. 1), and a fault complex similar in position to the Pernicana Fault. Fig. 6 shows the end results of

Fig. 6. Two analogue models of sand and plaster cones on a sand apron overlying a silicon putty basement sloping 2° towards the right, representing Mt. Etna's brittle summit cone and apron of lavas overlying the sloping ductile basement beneath it. Left and right images were taken 43 and 40 min respectively after the start of the experiments. Illumination is from the lower right in the left model, and from the upper right in the model on the right. Key parameters in both models are scaled to match those at Mt. Etna. The left model was a simple flared cone, whereas the right model was elongated north-south in an attempt to represent the Northeast rift and the Piano del Lago. The cone heights were 45 mm, the sand apron thinning from 20 mm beneath the cone to 8 mm to the right. The silicon thickness was 12 mm in the left model and 14 mm in the right model. Both models have a prominent summit graben complex that runs into a left-lateral strike-slip fault system similar to the Pernicana Fault on Etna (Fig. 1). Scale bar is 10 cm.

two experiments. Both models developed a prominent summit graben complex with faults and leaf graben at the southern end with similar orientations to fractures occurring over the 1983, 1985, 1991 and 2001 dykes observed and measured at the Piano del Lago, Schiena dell'Asino and the Serra Giannicola Grande, and also to the northeast-trending dykes at Portella Giumenta and the Valle del Leone. The origin of these features is discussed below in Section 5.3.

5. Discussion

5.1. Dyke intrusions

Most of the horizontal and vertical movement that has formed the summit graben has taken place during dyke injection at the start of fissure eruptions. In a perfect elastic medium, dyke injection causes the ground to be raised both sides of the dyke, and slightly lowered over the dyke itself (Dieterich and Decker, 1975, Pollard et al., 1983, Okada and Yamamoto, 1991). The overall effect is upward displacement that is permanent in the model situation, and the raised areas that remain at the southern end of the graben (Fig. 1) are all the remnants of uplifted ground adjacent to injected dykes, discussed below in Section 5.2. However, rocks behave elastically until they rupture, and in practice the driving pressure of the propagating dyke overcomes the tensile strength of the host rock, particularly when the dyke is near the surface. On Etna, this has occurred in every fissure and flank eruption, causing fracturing and the downfaulted areas 200 to 800 m wide that lie over the path of the dyke (e.g. Murray and Pullen, 1984; Murray, 1994). This downfaulting has resulted in an overall lowering of the surface at these locations, illustrated by the displacement of the benchmarks shown in Fig. 3. The north flank deformation during dyke injection has resulted in generally broader areas of fracturing and subsidence typically 2 km wide for the 7 dyke injection events described above (Fig. 3 left). This may indicate that the dykes intruded northward have been deeper than those on the south side. On the other hand these elastic models do not apply to intrusion into an extensional regime consequent upon downslope sliding of the edifice (Murray et al., 2018) as elaborated below. If extension is already occurring then less lateral pressure from intruding dykes is required to fracture the host rock, implying smaller raised areas. Whatever its cause, this broad subsidence over dykes on the north side often caused raised areas from previous dyke emplacements to subside (Murray et al., 1977; Murray, 1982; Murray, 1990; Bonaccorso et al., 2011), and the cumulative effect of these repeated subsidence events has been that no raised areas have been measured on the north side.

5.2. Areas of uplift

Eight of the high altitude stations shown in Fig. 1 show overall uplift, indicating a possible five areas where permanent uplift has occurred in the upper reaches of Mt. Etna, but only one of which has data for >40 years. The graphs of Fig. 7 (left) demonstrate how station 45a has shown subsidence during the 1983 eruption and particularly the 1991–3 eruption, when it subsided by more than a metre, but a small uprise of 0.2 m during the 1989 eruption and a major uprise of 1.5 m probably during the 2001 eruption, though the nail was lost under ash at this time and not found again until 2006. The station is a couple of hundred metres east of the 2001 dyke, so this episode of uprise was clearly an elastic response to pressure from the nearby dyke. Station DV in the Valle del Leone was situated about 100 m east of the 1989 fissure in the Valle del Leone, and had a remarkably large uplift of 2.06 m during this dyke emplacement for the same reason, but subsided 0.1 m over the following five years. Station B, on the Serra Giannicola Grande (Fig. 1) had smaller uplifts of 0.13 m during the 1985 eruption, a drop of 0.2 m in the 1989 eruption, and an uplift of 0.33 m at the start of the 1991–3 eruption. Both these uplifts were also apparently elastic responses to dyke injection, though in each case the distance from the dyke was of the order of a kilometre, so the uplift was correspondingly smaller.

Station IN (Fig. 7, right) was 500 m east of the 1983 dyke and about half that distance east of the 1985 dyke, and was in each event uplifted by about 0.25 m. The contrastingly greater uplift of DV and 45a stations is probably due to the steep slopes of the edge of the Valle del Bove and the Valle del Leone, which would have provided gravity assisted downslope movement on the eastern side of the dyke, adding to the magmatic pressure and causing correspondingly greater uplift. Station SS, situated at the very southern edge of the same area of uplift as IN, remained more or less stable from 1982 to 2000, after which it was unfortunately lost under the 2001 ash deposits. Stations XX, SR and Y,

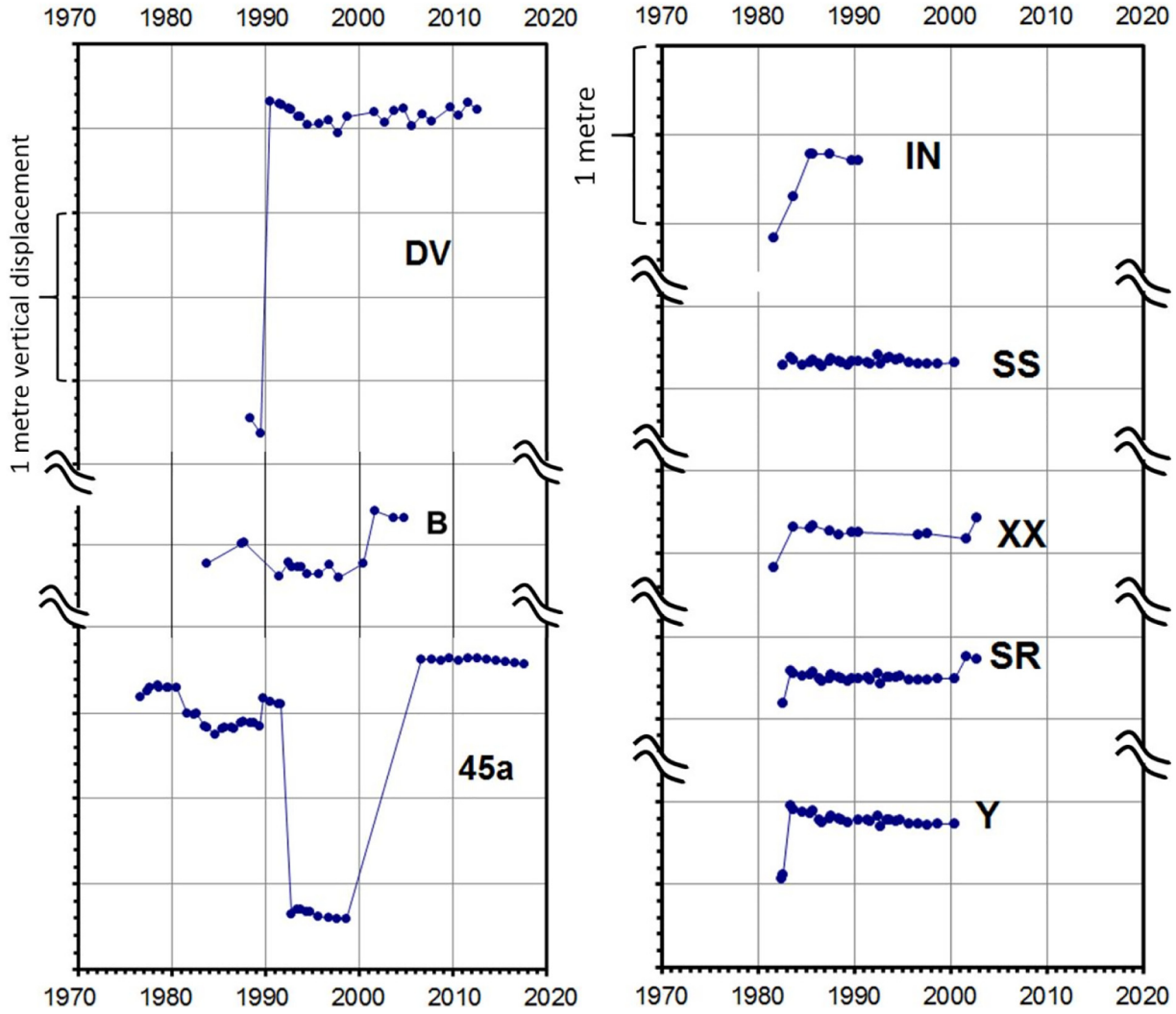

Fig. 7. Vertical displacements of the few stations that have shown overall uplift. Locations of stations are shown as white alphanumerics in Fig. 1. In every case, uplift has been caused by proximity to dyke intrusions during fissure eruptions, in some cases (DV, B and 45a) gravity assisted. See text for details.

situated on the western side of all the dyke intrusions in the southern rift, each experienced between 0.2 and 0.5 m of uplift in the 1983 event, followed by 0.1 m of subsidence over the following 7 or so years, but were almost unaffected by any other eruptions of the 1980s. Y was lost under 2001 ash, but XX and SR both rose just over 0.1 m during the 2001 eruption, after which they were buried under 2002–3 lava.

All areas of uplift were therefore the direct result of magma pressure from nearby dyke intrusions, in some cases gravity assisted, after which they often subsided of the order of 0.1–0.2 m over a period of 5 to 10 years.

5.3. Lava loading

Another factor that clearly has some influence on the graben subsidence is compaction of, and loading by, new lava flows. This causes subsidence of the new flow surface that is proportional to the depth of lava emplaced (Murray, 1988). Most of the benchmarks on the summit and north flank were installed on recent lavas dating from 1966 to 1981, whereas most of those on the south flank were initially installed on very old outcrops dating from 1787 or before. The most extreme case is the station at the Torre del Filosofo (TDF Figs. 1 & 3), on a building constructed in the 1950s over the site of a marble tower built in 125C.E. to celebrate the ascent of Etna by the Roman emperor Hadrian. Traces of this tower are still visible in 1943 air photographs, indicating that this benchmark is on deposits at least 1900 years old. The contrasting prevalence of recent lavas on the north flank might explain the greater amount of subsidence there between fissure eruptions. However, the cumulative measured subsidence that can be definitely attributed to lava flow compaction and loading rarely exceeds 0.1 m, except in the first year or two after emplacement, so subsidence here is still liable to be dominated by subsidence that occurs during dyke emplacement. Furthermore, it is noticeable that subsidence has continued between dyke injection events at a similar rate for thirty years 1987–2018 at north flank stations, rather than asymptotically declining as expected for compaction or loading.

Another interesting observation is the fact that the width of the graben has increased at a mean rate of up to 0.23 m yr^{-1} to 0.18 m yr^{-1} on the north & south flanks respectively at the same time as the graben subsided 0.08 m yr^{-1} to 0.06 m yr^{-1}. This width increase included displacements consequent upon the emplacement of at least 6 dykes on the north flank and 5 on the south. This north-south dyke emplacement suggests that east-west tensile stress was present throughout the 43-year period under study.

5.4. Gravitational spreading and downslope sliding

Analogue modelling of Etna and its surroundings provides clues to the origins of this tensile stress. Wooller et al. (2004) showed that

analogue models comprising a sand and plaster cone built on a sand apron and a silicon putty sloping basement produced movement of the cone downslope, and the consequent development of a summit graben striking normal to the direction of slope of the basement. This situation has been re-created in the models in Fig. 5, in which the parameters of the model have been scaled to match those at Mt. Etna. The origin of the summit graben appears to be the modification of the usual gravitational spreading of a cone by tensile stress induced by sliding of the entire cone down the basement slope. This sliding causes prefential formation of leaf graben normal to the basement slope, due to the increased tension in the direction of slope, and suppresses leaf graben on the upslope and downslope sides, emphasising the similar effects of buttressing by mountains on some sides of Etna (Merle and Borgia, 1996). The strike-slip fault complex mimicking the Pernicana fault most probably results from the obstruction of basement spreading along the top edge of the model by a sand ridge representing the Peloritani mountains immediately to the north and northeast of the volcano. This produces a relatively stable area on this side of the cone, to the left of point P in the lower part of Fig. 5, which contrasts with the free gravitational spreading of the cone and downslope creep of the basement towards the unbuttressed right hand edge. These conflicting stresses are resolved in the formation of a left-lateral strike-slip fault in the equivalent position of the Pernicana Fault. Some remnants of additional leaf graben are seen, particularly in the lower part of the first model, and at the top right of the second. These correspond to some of the fractures formed during the 1983, 1985, 1989, 1991–3 and 2001 eruptions.

The simple analogue models provide a clear explanation of why the summit graben, the Pernicana Fault, and the injected dykes have formed in their observed locations, shapes and orientations, but that is as far as the analogy can go. The injection of magma into the upper system of Etna, and the deposition of lava and pyroclastics at the surface are not represented by these simple models. The lateral pressure from dyke injection can cause fractures to open wider than would be the case from gravitational spreading and sliding, and produce compression and therefore increase sliding rates and gravitational spreading, at least locally. This could partially explain why the observed horizontal movement at Etna has been 2.7 to 3 times greater than the observed vertical subsidence. Another consequence of preferential dyke injection at these locations will be to concentrate lava emission at the graben edges or within them. This in turn will induce increased surface lava loading, and therefore greater compression and surface subsidence within the graben relative to surrounding areas.

Both these effects could be self-perpetuating, but the increased eruption incidence within and around the summit graben also has the effect of creating a topographic high connecting the summit to the Northeast Rift due to repeated lava accumulation. As intimated above, it also explains why the summit graben has escaped detection: it is persistently being covered by lava and pyroclastic deposits.

5.5. Summit graben at other volcanoes

Several volcanoes have developed summit graben under various circumstances more or less similar to those at Etna. On the very large scale, summit graben have developed at mid-ocean ridges such as the Juan de Fuca ridge and the East Pacific Rise (Macdonald and Fox, 1988, Lagabrielle and Cormier, 1999), under spreading rates 0.09 to 0.15 m y^{-1} (Fornari et al., 1998), about half what is observed here. These graben appear to develop in the same way as the Etna summit graben, from repeated dyke intrusions under a tensional regime, resulting in a dyke-induced graben structure, which is often then buried by lavas from subsequent eruptions (Chadwick and Embley, 1998). The Tharsis ridge on Mars, which lays claim to being the largest volcano in the solar system (Borgia and Murray, 2010), also has a major rift zone trending northeast-southwest across its summit and flanks. This might include a summit graben, though if so it has been buried beneath lava flows emanating from it, their source location being betrayed by a line of low hills connecting the northeast and the southwest rifts (Carr et al., 1977).

Mount St Helens developed a summit graben during its 1980 eruption, that formed during the asymmetric intrusion of a cryptodome, creating horizontal extension three orders of magnitude faster than that measured across the Etna summit graben (Moore and Albee, 1981), resulting in catastrophic sector collapse on that side. Donnadieu and Merle (1998) ran a series of analogue models suggesting that strike-slip faulting was the cause of this graben formation. However, Cecchi et al. (2005) examined the case of Casita volcano, Nicaragua, a hydrothermally altered and therefore weak-cored spreading volcano which also has a summit graben, and concluded that the slightly asymmetric deformation caused the summit graben by preferential spreading, and suggested the same was true of Mount St Helens. They also pointed out morphological features on Etna that suggest that this volcano might also have a weak core. They conclude that in any asymmetric volcano, preferential spreading occurs that can lead to graben development at the summit. Other volcanoes where summit graben have formed under gravitational spreading of the flanks are Poas and Turrialba, Costa Rica (Borgia et al., 1990). The Ardjuno and the Soropati-Telemojo volcanic complexes, Java, appear to be exact counterparts of the Etna situation, with summit graben systems that developed in response to gravitational spreading on a tilted substratum (Wooller et al., 2004).

6. Conclusions

It is concluded that an actively-forming sigmoidally-shaped graben measuring 1.5 × 9 km runs across the summit of Mt. Etna from south to north, where it joins the Pernicana Fault system. The graben floor is sinking at a mean rate of 0.07 m yr^{-1}, and the sides are extending laterally at a mean rate of 0.20 m yr^{-1}. Most of the graben lies hidden beneath the steadily accumulating lava flows and ash deposits, which have attained 120 m depth in places over the past 43 years, but its presence is revealed by those ground surveying stations or their witness points that have avoided burial.

Analogue modelling indicates that the graben system owes its position and configuration to a combination of gravitational spreading, which causes sinking at the summit and outward displacement of the flanks, and the downslope sliding of the entire edifice, which causes preferential extension in the downslope direction.

The subsidence is increased by the weight of new lava flows that are frequently extruded in the summit region and provide a continuously accumulating load on the floor of the graben, especially north of the summit where recent lavas are thickest.

The lateral extension of the graben is increased by magmatic pressure from dyke injection, that occurs preferentially along the faults and fissures produced by the spreading and sliding, and causes fractures to open wider than would be the case from gravitational spreading and sliding alone.

Traces of bounding faults in the 1932 topographical map of Etna indicate that this self-perpetuating process has been going on for longer than 400 years, and it is suggested that this repetitive sequence of events has continued and will continue throughout the lifetime of the volcano, and constitutes the principal eruption mechanism of Etna, and other volcanoes on Earth and Mars that share its diagnostic features.

Acknowledgements

I thank the 239 volunteer field assistants for their hard work and dedication to this project, and the Parco dell'Etna, the Corpo Forestale and the Aziende Foreste for the permission to work in their areas of jurisdiction, and also the Osservatorio Astrofisico (Catania) who gave permission to use their land for GPS, levelling and Dry Tilt stations. I am

grateful to the Ordnance Survey for donation of GPS equipment, to the Istituto Internazionale di Vulcanologia (Catania) for the loan of vehicles and equipment between 1981 and 1989, to the University of East London and University College London for the loan of equipment in 2001 and 2011, and to Ben van Wyk de Vries and Martino Claudia for instruction and assistance with the laboratory analogue modelling in 2018. I am also grateful to T. J. Sanderson for providing altitudes of benchmarks of the Flank Levelling Traverse in 1980 and 1981, and to M. Breach for converting the individual trilateration distances and vertical angles measured between 1987 and 1994 into spherical xyz coordinates with STAR*NET - PRO. This work was supported by U.K. Natural Environment Research Council (NERC) grants NER/A/S/2001/00686, NER/A/S/2002/00411, NER/A/S/2003/00105, NE/D001390/1, NE/E007589/1, and 4 previous NERC grants 1975-77, 1977-80, 1987-88 & 1995-97, also 5 CNRS (France) grants 1982, 1983, 1984, 1985, 1986, 2 NATO grants 1987-89 & 1989-1991, 3 European Union grants ERB40002PL900491-(90400491), EV5V-CT92-0170 & ENV4-CT96-0294, a Leverhulme Trust (U.K.) grant 1995-98, 3 Open University (U.K.) Research grants 1990, 1991 & 1998-2000, and by NERC GEF loan Nos. 727, 776, 799, 825 and 869. Since 2008 this project has been entirely self-funded through the kind generosity of 68 field assistants. I am grateful to Dr. Frances Jenner and Dr. Anne Jay who read the manuscript and provided many helpful improvements, and to 2 anonymous reviewers who suggested many additions that have greatly improved the quality of the paper.

Appendix A. Supplementary data

Supplementary data to this article can be found online at https://doi.org/10.1016/j.jvolgeores.2019.07.024.

References

Behncke, B., Neri, M., Pecora, E., Zanon, V., 2006. The exceptional activity and growth of the Southeast Crater, Mount Etna (Italy), between 1996 and 2001. Bull. Volcanol. 69, 149–173. https://doi.org/10.1007/s00445-006-0061-x.

Bonaccorso, A., 1999. The March 1981 Mount Etna eruption inferred through ground deformation modelling. Phys. Earth Planet. Inter. 112, 125–136.

Bonaccorso, A., Bonforte, A., Calvari, S., Del Negro, C., Di Grazia, G., Ganci, G., Neri, M., Vicari, A., Boschi, E., 2011. The initial phases of the 2008–2009 Mount Etna eruption: a multidisciplinary approach for hazard assessment. J. Geophys. Res. 116 (B03203, doi:10.1029/2010JB007906).

Bonforte, A., Guglielmino, F., 2015. Very shallow dike intrusion and potential slope failure imaged by ground deformation: the 28 December 2014 eruption on Mount Etna. Geophys. Res. Lett. 42, 2727–2733. https://doi.org/10.1002/2015GL063462.

Bonforte, A., Guglielmino, F., Coltelli, M., Ferretti, A., Puglisi, G., 2011. Structural assessment of Mount Etna volcano from permanent scatterers analysis. Geochem. Geophys. Geosyst. 12. https://doi.org/10.1029/2011GC003213.

Borgia, A., Murray, J.B., 2010. Is Tharsis Rise, Mars, a spreading volcano? Geological Society of America Special Paper 470, 115–122.

Borgia, A., Burr, J., Montero, W., Morales, L.D., Alvarado, G.E., 1990. Fault propagation folds induced by gravitational failure and slumping of the central Costa Rica volcanic range: implications for large terrestrial and Martian volcanic edifices. J. Geophys. Res. 95, 14357–14382.

Borgia, A., Ferrari, L., Pasquaré, G., 1992. Importance of gravitational spreading in the tectonic and volcanic evolution of Mount Etna. Nature 357, 231–235.

Branca, S., Ferrara, V., 2013. The morphostructural setting of Mount Etna sedimentary basement (Italy): Implications for the geometry and volume of the volcano and its flank instability. Tectonophysics 586, 46–64. https://doi.org/10.1016/j.tecto.2012.11.011.

Briole, P., Gaulon, R., Nunnari, G., Puglisi, G., Ruegg, J.C., 1992. Measurements of ground movement on mount etna, sicily: a systematic plan to record different temporal and spatial components of ground movement associated with active volcanism. In: Gasparini, P., Scarpa, R., Aki, K. (Eds.), Volcanic Seismology. IAVCEI Proceedings in Volcanology. vol. 3. Springer, Berlin, Heidelberg.

Carr, M.H., Greeley, R., Blasius, K.R., Guest, J.E., Murray, J.B., 1977. Some martian volcanic features as viewed from the Viking Orbiters. J. Geophys. Res. 82, 3985–4015.

Cecchi, E., van Wyk de Vries, B., Lavest, J.M., 2005. Flank spreading and collapse of weak-cored volcanoes. Bull. Volcanol. 67, 72–91.

Chadwick, W.W., Embley, R.W., 1998. Graben formation associated with recent dike intrusions and volcanic eruptions on the mid-ocean ridge. J. Geophys. Res. 103 (B5), 9807–9825.

Dieterich, J.H., Decker, R.W., 1975. Finite element modelling of surface deformation associated with volcanism. J. Geophys. Res. 80, 4094–4102.

Donnadieu, F., Merle, O., 1998. Experiments on the indentation process during cryptodome intrusions: New insights into Mount St. Helens deformation. Geology 26 (1), 79–82.

Ferrucci, F., Rasá, R., Gaudiosi, G., Azzaro, R., Imposa, S., 1993. Mt. Etna: a model for the 1989 eruption. J. Volcanol. & Geotherm Res. 56, 35–56.

Fornari, D.J., Haymon, R.M., Perfit, M.R., Gregg, T.K.P., Edwards, M.H., 1998. Axial summit trough of the East Pacific Rise 9°N to 10°N: Geological characteristics and evolution of the axial zone on fast-spreading mid-ocean ridges. J. Geophys. Res. 103 (B5), 9827–9855.

Guest, J.E., Murray, J.B., 1979. An analysis of hazard from Mt. Etna Volcano. J. Geol. Soc. Lond. 136, 347–354.

Hamilton, W., 1770. An account of a journey to Mount Etna, in a letter from the Honourable William Hamilton, His Majesty's Envoy Extraordinary at Naples, to Matthew Maty, M.D. Sec. R.S. *Phil. Trans. Roy Soc.* Lond. 60, 1–19.

Lagabrielle, Y., Cormier, M.-H., 1999. Formation of large summit troughs along the East Pacific Rise as collapse calderas: an evolutionary model. J. Geophys. Res. 104 (B6), 12971–12988.

Lanzafame, G., Neri, M., Acocella, V., Billi, A., Funiciello, R., Giordano, G., 2003. Structural features of the July-August 2001 Mount Etna eruption: evidence for a complex magmatic system. J. Geol. Soc. Lond. 160, 531–544.

Macdonald, K.C., Fox, P.J., 1988. The axial summit graben and cross-sectional shape of the East Pacific rise as indicators of axial magma chambers and recent volcanic eruptions. Earth Planet. Sci. Lett. 88, 119–131.

McGuire, W.J., Murray, J.B., Pullen, A.D., Saunders, S.J., 1991. Ground deformation at Mt Etna; evidence for dyke emplacement and slope instability. J. Geol. Soc. Lond. 148, 577–583.

Merle, O., Borgia, A., 1996. Scaled experiments of volcanic spreading. J. Geophys. Res. 101 (B6), 13, 805–13, 817.

Moore, J.G., Albee, W.C., 1981. Topographic and structural changes, March–July 1980: photogrammetric data. United States Geological Survey Professional Paper 1250. The 1980 Eruptions of Mount St Helens, Washington. United States Government Printing Office, Washington D.C., pp. 123–134.

Murray, J.B., 1980. Map of the summit area of Mt Etna in September 1978. UK Research on Mt Etna 1977–1979. R Soc Lond 33–36.

Murray, J.B., 1982. Les déformations de l'Etna à la suite de l'éruption de Mars 1981. Bulletin PIRPSEV No 57. pp. 1–30.

Murray, J.B., 1988. The influence of loading by lavas on the siting of volcanic eruption vents on Mt Etna. J. Volcanol. & Geotherm. Res. 35, 121–139.

Murray, J.B., 1990. High-level Magma Transport at Mt Etna Volcano, as Deduced from Ground Deformation Measurements. Chapter 17 of Magma Transport & Storage, Ed. Ryan, John Wiley & Sons Ltd., pp 357–383.

Murray, J.B., 1994. Elastic model of the actively intruded dyke feeding the 1991–1993 eruption of Mt Etna, derived from ground deformation measurements. Acta Vulcanologia 4, 97–99.

Murray, J.B., Guest, J.E., 1982. Vertical ground deformation in Mount Etna, 1975-1980. Geol. Soc. Am. Bull. 93, 1160–1175.

Murray, J.B., Pullen, A.D., 1984. Three-dimensional model of the feeder conduit of the 1983 eruption of Mt Etna volcano, from ground deformation measurements. Bull. Volcanol. 47 (4 (2)), 1145–1163.

Murray, J.B., Guest, J.E., Butterworth, P.S., 1977. Large ground deformation on Mt Etna Volcano. Nature 266, 338–340.

Murray, J.B., Décobecq, D., Bond, A.J., 1989. L'éruption paroxysmale du Cratère Nord-est de l'Etna du 24 septembre 1986. L'Association Volcanologique Européene, pp. 11–23 No. 22.

Murray, J.B., Voight, B., Glot, J.-P., 1994. Slope movement crisis on the east flank of Mt Etna volcano: Models for eruption triggering and forecasting. Eng. Geol. 38, 245–259.

Murray, J.B., Pullen, A.D. & Saunders, S. 1995. Ground Deformation Surveying of Active Volcanoes. Chapter 5 of Monitoring Active Volcanoes: Strategies, Procedures, Techniques. Ed. McGuire, W.J., Kilburn, C.R.J. & Murray, J.B., pp. 113–150.

Murray, J.B., van Wyk de Vries, B., Pitty, A., Sargent, P.T.H. & Wooller, L.K. 2018. Gravitational sliding of the Mt. Etna massif along a sloping basement. Bull. Volcanol. 80: 40. doi:https://doi.org/10.1007/s00445-018-1209-1.

Neri, M., Acocella, V., Behncke, B., 2004. The role of the Pernicana Fault System in the spreading of Mount Etna (Italy) during the 2002–2003 eruption. Bull. Volcanol. 66, 417–430. https://doi.org/10.1007/s00445-003-0322-x.

Nunnari, G., Puglisi, G., 1994. Ground deformation studies during the 1991–93 Etna eruption using GPS data. Acta Vulcanologia. 4, 101–108.

Obrizzo, F., Pingue, F., Troise, C., De Natale, G., 2001. Coseismic displacements and creeping along the Pernicana fault (Mt. Etna, Italy) in the last 17 years: a detailed study of a tectonic structure on a volcano. J. Volcanol. Geotherm. Res. 109, 109–131.

Okada, Y., Yamamoto, E., 1991. Dyke Intrusion Model for the 1989 Seismovolcanic Activity off Ito, Central Japan. J. Geophys. Res. 96 (B6), 10361–10376.

Pollard, D.D., Delaney, P.T., Duffield, W.A., Endo, E.T., Okamura, A.T., 1983. Surface deformation in volcanic rift zones. Tectonophysics 94, 541–584.

Ruch, J., Pepe, S., Casu, F., Solaro, G., Pepe, A., Acocella, V., Neri, M., Sansosti, E., 2013. Seismo-tectonic behavior of the Pernicana Fault System (Mt Etna): a gauge for volcano flank instability? J. Geophys. Res. Solid Earth 118, 4398–4409. https://doi.org/10.1002/jgrb.50281.

Rymer, H., Murray, J.B., Brown, G.C., Ferrucci, F., McGuire, W.J., 1993. Mechanisms of magma eruption and emplacement at Mt Etna between 1989 and 1992. Nature 361, 439–441.

Sanderson, T.J.O., Berrino, G., Corrado, G., Grimaldi, M., 1983. Ground deformation and gravity changes accompanying the March 1981 eruption of Mount Etna. J. Volcanol. & Geoth. Res. 16, 299–315.

Sargent, P.T.H., Murray, J.B., 1994. GPS Joins the Mt Etna Monitoring Programme. vol. 19. Civil Engineering Surveyor, pp. 14–17 No. 9.

Sartorius von Waltershausen, W., 1880. Der Aetna. Liepzig, Engelman.
Tanguy, J.C., 1981. Les éruptions historiques de l'Etna: chronologie et localisation. Bull. Volcanol. 44, 585–640.
Villari, L., 1977. How Do the Summit of Mt Etna Deform during Persistent Activity?. Open file report 1/77. I.I.V.-C.N.R, Catania, Italy
Villari, L.Ed., 1983. 1981 Etna Report. Open file report 2/83. I.I.V.-C.N.R, Catania, Italy.
Wadge, G., 1976. Deformation of Mt Etna 1971-1974. J. Volcanol. & Geotherm. Res. 1, 237–263.
Wooller, L.K., van Wyk de Vries, B., Murray, J.B., Rymer, H., Meyer, S., 2004. Volcano spreading controlled by dipping substrata. Geology 32 (7), 573–576. https://doi.org/10.1130/G20472.